Fluoride Ion Interactions in Alkali Metal Fluoride-Diol Complexes

Yuto Tonouchi,[†] *Kazuhiko Matsumoto,**[,†] *Takashi Nagata,*[‡] *Masato Katahira,*[‡] *and Rika Hagiwara*[†]

[†]Graduate School of Energy Science, Kyoto University, Yoshida, Sakyo-ku, Kyoto, 606-8501, Japan, [‡]Institute of Advanced Energy, Kyoto University, Gokasho, Uji, Kyoto 611-0011, Japan

ABSTRACT

The activity of F^- is an important factor in the design of both inorganic and organic reactions involving fluorine-compounds. The present study investigates interactions of F^- with diols in alkali metal fluoride-diol complexes. Increases in the reactivities of alkali metal fluorides and their solubilities in alcohols is observed with increasing cation size. The difference in alkali metal ion size produces different structural motifs for F^--diol complex salts. The CsF complex salt with ethylene glycol (EG), CsF-EG, has a layered structure, whereas the Rb and K complex salts, $(RbF)_5$-$(EG)_4$ and $(KF)_5$-$(EG)_4$, form columnar structures. Comparison of the CsF complex salts with three different diols, EG, 1,3-propylene glycol (PG_{13}), and 1,4-butylene glycol (PG_{14}), revealed that the diol chain length affects the bridging mode in their layered structures. EG bridges two OH oxygen atoms within the same CsF layer in CsF-EG, whereas PG_{13} and BG_{14} bridge two OH oxygen atoms in different CsF layers in $(CsF)_2$-PG_{13} and CsF-BG_{14}, respectively. The F^- ion coordination environment involves interactions between alkali metal ions and H atom(s) in the diol OH groups, where the $F^-\cdots H$ interactions are more dominant than the $F^-\cdots M^+$ interaction based on Hirshfeld surface analyses. The O−H bond weakening observed by infrared spectroscopy also reflects the strengths of the $F^-\cdots H$ interactions in these complex salts.

INTRODUCTION

The chemistry of naked fluoride has a long history. Strictly speaking, "naked" fluoride ion exists only in vacuum, because it is influenced by solvent or counterions under ordinary circumstances.[1-4] However, in combination with a large cation, F^- is often regarded as naked, because its ability to surround itself with other entities decreases with increasing cation size.[3] Although cesium fluoride is sometimes used to produce reactive F^- owing to the large cation-to-anion ratio (cesium effect),[2,3] the size of Cs^+ is still insufficient for certain purposes. Several attempts have been made to prepare F^- salts with an organic cation. Christe and co-workers reported the first truly stable anhydrous organic cation fluoride salt by dehydrating tetramethylammonium fluoride ([TMA]F).[1] Subsequently, several organic cations have been combined with F^- including tetrabutylammonium ([TBA]F),[4] *N*-methylquinuclidinium,[5] tetramethylphosphonium,[6] ([TMP]F), and $(L^{Dipp})H^+$ (L^{Dipp} = 1,3-bis(2,6-diisopropylphenyl)-1,3-dihydro-2H-imidazol-2-ylidene)[7].[8-11]

Reactive and highly basic F^- combined with an organic cation is often used to increase the solubility of an inorganic fluorocomplex or to stabilize the anion of a weakly Lewis acidic parent fluoride (weak fluoride ion acceptor).[12-24] Different aspects must be considered in organic fluorination reactions. Fluoride ion reactivity is desirable in substitution reactions, but high basicity can lead to elimination reactions and reduces S_N2/E2 selectivity.[25,26] Most organic cations are unstable when combined with F^-. Such salts are hard to isolate due to β-hydrogen elimination,[1,27-29] although this can be avoided with [TMA]F because the β-hydrogen atoms are absent (as in the exceptional case of *N*-methylquinuclidinium salt)[5]. Reactive anhydrous F^- is sometimes created in an unusual way, as in the in situ generation of [TBA]F from hexafluorobenzene and [TBA]CN.[4] Organic fluoride salts can be stabilized as hydrates, but the

quality of “nakedness” is lost in such cases and even a trace of water is not preferable under certain conditions due to the high reactivity of H_2O.[1,30]

Taming F^- with a hydrogen-bond donor is an effective and practical approach, because F^- basicity can be moderated by hydrogen bonding, thereby preventing its attack on organic cations and allowing preferable reactivity to be tuned.[25,31] An early application of this strategy demonstrated that introduction of alcohols as hydrogen-bond donors to [TBA]F leads to high reactivity in S_N2 fluorination reactions.[32] This work also revealed alcohol-induced steric effects on reactivity, which were confirmed by the X-ray crystal structure of [TBA]F-(*t*-BuOH)$_4$. In subsequent publications, enhanced kinetic reactivity and S_N2/E2 selectivity were reported using CsF and bulky alcohols.[33-35] The effects of the F^- coordination mode on nucleophilic reactivity were investigated for a number of fluoride-alcohol complexes using [TBA]F as a fluoride-ion source.[26,36] Insights derived from crystal structures revealed that the alcohol coordination number was closely linked to reactivity. A related topic is fluoride-ion solvation by ionic liquids. An equimolar mixture of ethylene glycol (EG) and [1-ethyl-3-methylimidazolium]F forms a stable ionic-liquid solvate that exhibits a strong $F^-\cdots$EG interaction, yet is functional in a nucleophilic substitution reaction.[37]

Further understanding, including crystallographic insight, is needed to characterize the interactions between F^- and alcohols in fluoride-alcohol complexes. Although nuclear magnetic resonance spectroscopy is useful in discerning solution state properties, a previous study has determined that the ^{19}F NMR chemical shift is not a good measure of F^- nakedness either in solution or in the solid state because of solvent-induced paramagnetic shielding.[38] Currently known crystal structures of fluoride-alcohol complexes are limited to [TBA]F salts with *t*-BuOH,[39] 1-adamantanol,[26] pentaerythritol,[26] tris(hydroxymethyl)ethane,[26] neopentylglycol,[26]

(*R*,*R*)-di-(*i*-Pr)-tartrate,[26] a mannitol derivative,[26] pinacol,[26] (*R*)-BINOL,[26] cyclic hemiacetal,[26] 9-phenylfuoren-9-ol,[26] diphenylmethanol,[26] triphenylmethanol,[26] tri-(p-tolyl)-methanol,[26] pyrrolidine,[26] large phenol derivatives[40] and a [TEA]F salt with BINOL.[41] Contrary to expectations, alcohol complexes with alkali metal fluorides have scarcely been investigated, especially by X-ray crystallography. Although alkali metal fluorides do not possess the high organic solvent solubilities and fluorinating capabilities of alkylammonium fluorides, their ease of use and low cost are attractive for many practical applications. This contrasts with the extensive exploration of fluoride-urea derivative complexes by X-ray and neutron single-crystal diffraction,[31,42-45] where intermolecular H···F^- interactions are known to be important.

The present work investigates the interactions between F^- and OH groups in alkali metal fluoride–diol systems. Basic reactivity and solubility studies are described in the first part. Single-crystal X-ray diffraction analyses are possible owing to the relatively high solubilities and reactivities of KF, RbF, and CsF salts in EG. The crystal packing and coordination environments of F^- are categorized based on differences in cation size (K^+, Rb^+, and Cs^+) and the diol alkyl chain length of EG, 1,3-propylene glycol (PG_{13}), and 1,4-butylene glycol (BG_{14}). Spectroscopic analysis is used probe intermolecular interactions. The subsequent discussion provides useful insight to the solution structure and reactivity of F^- including the possible application of alkali metal fluorides in alcohols for organic and inorganic reactions.

RESULTS AND DISCUSSION

Reactivity of alkali metal fluorides and EG. The reactivities of alkali metal fluorides and EG were characterized in terms complex salt formation in the solid state. Table 1 summarizes the complex-forming ability of alkali metal fluorides with EG. Mixtures of alkali metal fluorides and

EG were stirred for one week at 25 °C. Complex formation was evaluated from changes in the X-ray powder diffraction (XRPD) patterns (Figures S1 and S2, Supporting Information). The same procedure was followed with ethanol (EtOH). EG forms complex salts with KF, RbF, and CsF, whereas EtOH forms a complex salt with only CsF. This trend in behavior is explained by an increase in Lewis basicity of F^- with increasing the size of counterion.[2,3] The greater complex forming ability of EG relative to EtOH is attributable to the double coordination sites on each EG molecule.

Alkali metal fluoride solubility in EG or EtOH is a good indicator of reactivity, because F^--(alcohol)$_n$ complexes form upon dissolution. Table 1 lists alkali metal fluoride solubilities in EG and EtOH measured by X-ray fluorescence spectroscopy (XRF). The XRF results suggest that solubilities of alkali metal fluorides in EG increases sharply between NaF and KF and thereafter slightly in the order KF < RbF < CsF. These results prompted us to focus on the structural analyses of alkali metal fluoride-diol complexes. The samples for ^{1}H NMR measurements (0.1 mol dm^{-3} EG solutions of KF, RbF, and CsF) were prepared by simply dissolving the corresponding alkali metal fluoride in EG. The resulting ^{1}H NMR chemical shifts are similar to each other and to that of pure EG because of the low alkali fluoride concentration (Figure S3, Supporting Information). The ^{1}H NMR spectra of the alkali metal fluoride EG complexes, whose structures will be discussed below, were not measured in this work because of their low solubilities in aprotic solvents (e.g., below 0.005 mol dm^{-3} for CsF· EG in typical solvents including *N*,*N*-dimethylformamide, tetrahydrofuran, difluorobenzene, and acetonitrile). The ^{19}F NMR chemical shift of ca. −136 ppm (Figure S4, Supporting Information) is cation independent, which agrees with previous reports that this chemical shift depends on the solvent and not on the

Table 1. Reactivity and solubility of alkali metal fluorides with EG and EtOH.[a]

	EG		EtOH	
	Reactivity	Solubility (mol dm^{-3})	Reactivity	Solubility (mol dm^{-3})
LiF	No reaction	<0.10	No reaction	<0.10
NaF	No reaction	<0.10	No reaction	<0.10
KF	Complex formed	0.33	No reaction	<0.10
RbF	Complex formed	0.38	No reaction	0.38
CsF	Complex formed	0.45	Complex formed	0.45

[a] Complex formation was confirmed by the change in XRPD patterns (see Figures S1 and S2, Supporting Information). Solubility was measured by XRF.

counterion (*ca.* −137 ppm in EtOH and −147 ppm in MeOH for KF, CsF, [TMA]F, and [TMP]F).[6,38]

X-ray Crystal Structures. Crystallographic data for CsF-EG, $(RbF)_5$-$(EG)_4$, $(KF)_5$-$(EG)_4$, $(CsF)_2$-PG_{13}, and CsF-BG_{14} at 113K are provided in Table 2. Single crystals of CsF-EG were grown from its tetraglyme solution after standing at room temperature, and other crystals were recrystallized by slowly cooling the corresponding saturated diol solution from an elevated temperature to room temperature. Selected bond lengths and angles appear in the structural diagrams. Other geometrical parameters are listed in Table S1. Hydrogen-bonding geometries are listed in Table 3. Individual bond valences were evaluated to determine the contribution of each contact to the bond valence sum (BVS) for the alkali metal cation (see Table S2 for details of BVS calculations).[47,48]

Figure 1 shows the packing diagrams of CsF-EG and $(RbF)_5$-$(EG)_4$. Because the Rb and K salts, $(RbF)_5$-$(EG)_4$ and $(KF)_5$-$(EG)_4$, are isostructural with each other, only the $(RbF)_5$-$(EG)_4$

structure is described here. The CsF-EG complex is best described as a layered structure with alternate polar (Cs^+, F^-, and −OH) and non-polar (−CH_2−CH_2−) layer stacking (Figure 1a). The $Cs^+\cdots F^-$, $Cs^+\cdots O$, and $F^-\cdots H$ contacts are the main interactions in the polar region with EG bridging to the F^- ions in the same layer. These interactions lead to a gauche conformation for EG with a dihedral angle of −61.4(5)°, similar to that found for pure EG.[49,50] The EG molecules are interact via van der Waals interactions in the nonpolar region along the *c*-axis. Consideration of the primary and secondary contacts with Cs^+ (three F^- and six O atoms in

Table 2. Summary of crystallographic data and refinement results for CsF-EG, $(RbF)_5$-$(EG)_4$, $(KF)_5$-$(EG)_4$, $(CsF)_2$-PG_{13}, and CsF-BG_{14}.

	CsF-EG	$(RbF)_5$-$(EG)_4$	$(KF)_5$-$(EG)_4$	$(CsF)_2$-EG	CsF-BG_{14}
Formula	$CsFC_2H_6O_2$	$Rb_5F_5C_8H_{24}O_8$	$K_5F_5C_8H_{24}O_8$	$Cs_2F_2C_3H_8O_2$	$CsFC_4H_{10}O_2$
fw	213.98	770.62	538.77	379.91	242.03
T / K	113	113	113	113	113
cryst system	orthorhombic	tetragonal	tetragonal	orthorhombic	monoclinic
space group	*Pbca*	*P*4/*n*	*P*4/*n*	*Immm*	$P2_1/c$
a / Å	7.5822(3)	13.6999(9)	13.2866(6)	4.1727(4)	4.6451(4)
b / Å	8.4230(4)	13.6999(9)	13.2866(6)	4.4285(4)	7.8792(6)
c / Å	17.1081(9)	5.9083(4)	5.8173(3)	23.915(2)	20.1103(17)
β/ °	90	90	90	90	93.032(3)
V / Å^3	1092.87(9)	1108.91(16)	1026.95(11)	441.92(7)	735.00(10)
Z	8	2	2	2	4
ρ_{calc} / g cm^{-3}	2.601	2.308	1.742	2.855	2.187
μ / mm^{-1}	6.678	11.024	1.144	8.222	4.979
R_1[a]	0.0348	0.0332	0.0236	0.0198	0.0206
wR_2[b]	0.0866	0.0794	0.0602	0.0479	0.0496
cryst size / mm^3	0.30×0.20×0.10	0.30×0.30×0.30	0.30×0.20×0.20	0.20×0.10×0.10	0.20×0.15×0.10

[a] $R_1 = \Sigma||F_o| - |F_c||/\Sigma|F_o|$. [b] $wR_2 = [\Sigma w(F_o^2 - F_c^2)^2/\Sigma w(F_o^2)^2]^{1/2}$.

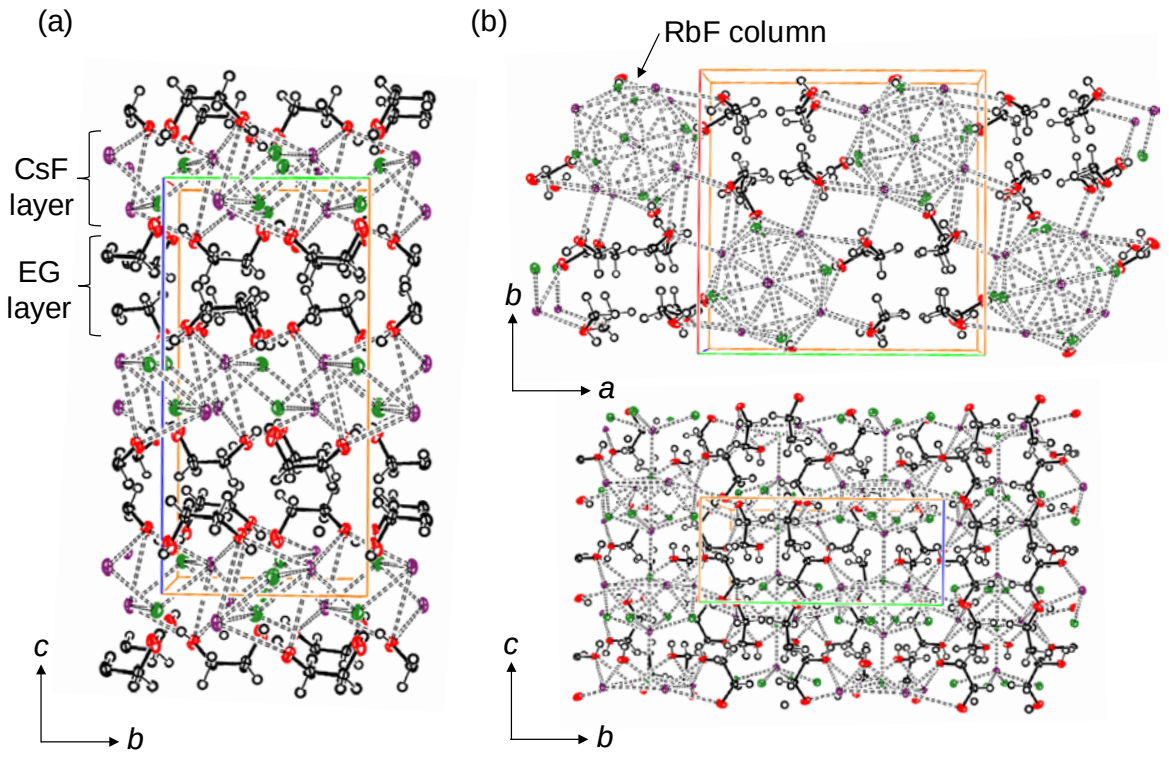

Figure 1. Packing diagrams of (a) CsF-EG viewed along the *a*-axis and (b) $(RbF)_5$-$(EG)_4$ along the *c*- and *a*-axes. Atom colors: C and H, black; O, red; F, green; Cs and Rb, purple. Hydrogen bonds are not shown for clarity.

EG) yields a BVS of 1.03 as expected for Cs(I) [see Figure S5a, Supporting Information, for the coordination environment of Cs^+ in CsF-EG]. The packing mode of $(RbF)_5$-$(EG)_4$ is columnar, where the $Rb^+\cdots F^-$ interaction forms the main framework for the columns which have rock salt-type arrangements of ions. These columns are mutually connected through EGs by means of $Rb^+\cdots O$ and $F^-\cdots H$ interactions (Figure 1b). The O−C−C−O dihedral angle in EG is 68.6(3)° is similar to that in CsF-EG above. There are no hydrogen-bond interactions between the EG molecules. There are two crystallographically independent Rb^+ ions (one along the central axis

and the other at the column edge) that have significantly different BVS values. The Rb1 cation has a BVS of 1.11, which suggests an over-coordinated environment relative to a BVS of 1.01 for Rb2 [see Figure S5b, Supporting Information, for the coordination environment of Rb^+ in $(RbF)_5$-$(EG)_4$]. Considering a similar trend in the isostructural K^+ salt [BVS = 1.05 for K1 and 0.93 for K2 in $(KF)_5$-$(EG)_4$], the alkali metal site at the edge of the column is more crowded owing to multiple contacts with the O atoms of EG outside the column.

Figure 2 shows the coordination environment of F^- in CsF-EG and $(RbF)_5$-$(EG)_4$. The F^- ion in CsF-EG is coordinated to three Cs^+ ions and two H atoms of OH groups in different EG molecules. In contrast, $(RbF)_5$-$(EG)_4$ has two crystallographically independent F^- ions. The F1 anion outside the column is similar to F^- in CsF-EG and is coordinated by three Rb^+ ions and two H atoms from OH groups in different EG molecules. The F2 anion inside the column is coordinated to six Rb^+ ions in a distorted octahedral environment. The Cs···F^- contacts 2.946(3), 2.980(3), and 3.034(3) Å in CsF-EG are similar, on average, to that in the rock salt-type CsF structure (3.004 Å).[51,52] The Rb···F distances around F1 in $(RbF)_5$-$(EG)_4$ are also similar, on average, to that in the rock salt-type

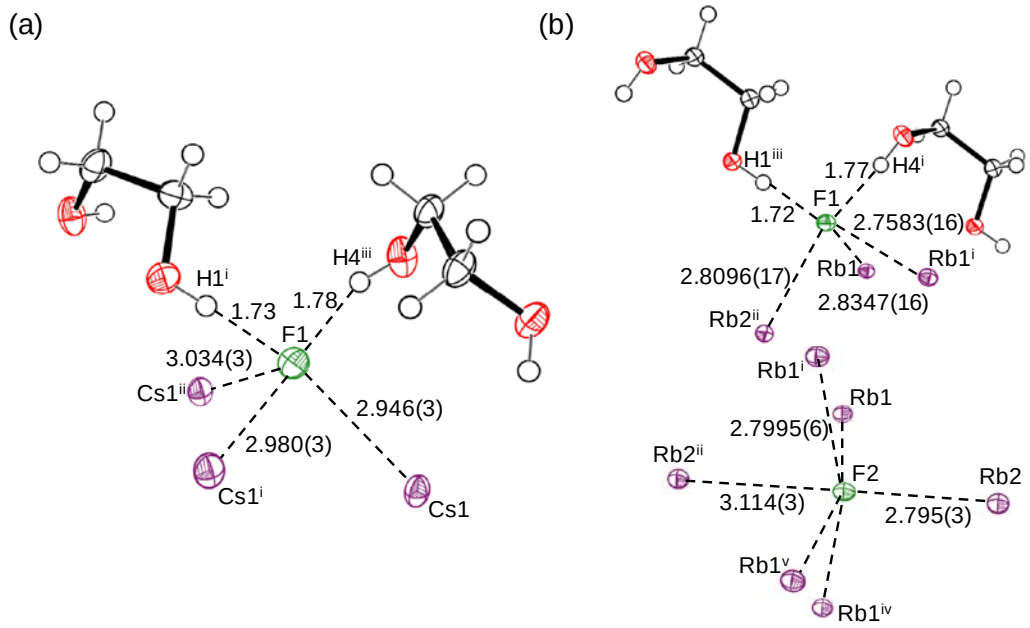

Figure 2. Coordination environments of F^- in (a) CsF-EG [symmetry code: (i) x+1/2, −y+2/3, −z+1; (ii) −x+1/2, y−1/2, z; (iii) −x, −y+2, −z+1] and (b) $(RbF)_5$-$(EG)_4$ [symmetry code: (i) y, −x+2/3, z; (ii) y+1/2, −x+3/2, z+1; (iii) x, y, z+1; (iv) −y+3/2, x, z; (v) −x+3/2, −y+2/3, z]. Thermal ellipsoids are shown at the 50 % probability level. Contact distances are shown in Å.

RbF structure (2.815Å)[51,52] although the range of values is larger (2.7583(16), 2.8096(17), and 2.8347(16) Å). The F2 anion in the distorted FRb_6 octahedron displays short and long Rb2···F2 contacts (2.795(3) and 3.114(3) Å) along the central axis of the column and four equivalent Rb1···F2 contacts of 2.7995(6) Å. The short H···F interaction distances, 1.73 and 1.78 Å in CsF-EG and 1.72 and 1.77 Å in $(RbF)_5$-$(EG)_4$ (Table 3) indicate the formation of strong hydrogen bonds based on the van der Waals interaction sum of 2.7 Å.[53] It should be noted that even the corresponding O(H)···F^- distances (2.538(3) to 2.579(3) Å with an O−H···F^- angle >158.2°), listed in Table 3, are all shorter than this value. A shorter H···F distance is observed in fluoride-alcohol complexes with a bulky cation [e.g., 1.66 Å in $([C_2C_1im]F)_2$-EG], where F^- is coordinated to one H atom from

Table 3. Hydrogen bonding geometries (Å, °) in CsF-EG, $(RbF)_5$-$(EG)_4$, $(KF)_5$-$(EG)_4$, $(CsF)_2$-PG_{13}, and CsF-BG_{14}.

	O−H	H···F	O···F	O−H···F
CsF-EG				
O1−H1···F1	0.82	1.73	2.549(4)	177.6
O4−H4···F1	0.82	1.78	2.559(4)	158.2
$(RbF)_5$-$(EG)_4$				
O1−H1···F1	0.82	1.72	2.538(3)	173.4
O4−H4···F1	0.82	1.77	2.579(3)	168.0
$(KF)_5$-$(EG)_4$				
O1−H1···F1	0.82	1.74	2.5638(11)	178.4
O4−H4···F1	0.82	1.78	2.5961(11)	171.0
$(CsF)_2$-PG_{13}				
O1−H1···F1	0.82	1.69	2.469(6)	158.6
CsF-BG_{14}				
O1−H1···F1	0.82	1.72	2.524(2)	166.2
O6−H6···F1	0.82	1.73	2.541(2)	169.3

an OH group and three aromatic H atoms of the $C_2C_1im^+$ cation.[37] The F^- ions that are coordinated to only H atoms of OH groups often have a longer contact distance [e.g., 1.83 Å in [TBA]F-(^{t}BuOH)$_4$, where F^- is tetrahedrally coordinated to four H atoms of OH groups].[54]

Figure 3 shows the packing diagrams of $(CsF)_2$-PG_{13} and CsF-BG_{14}. The PG_{13} molecules in $(CsF)_2$-PG_{13} are positionally disordered into two sites by a crystallographic mirror plane. These two complex salts have layered structures with alternate polar and non-polar layers. Although CsF-EG also has a layered structure, the configuration of the constituent ions and diols in CsF-EG, $(CsF)_2$-PG_{13}, and CsF-BG_{14} differ from each other. The PG_{13} and BG_{14} molecules bridge F^- ions between two different polar layers, whereas EG bridges F^- ions within the same layer. This suggests that the bridging mode depends on the diol chain length, because long alkyl

chains tend to be aligned by van der Waals interactions. The structures of the polar layers containing Cs^+ and F^- ions differ for $(CsF)_2$-PG_{13} and CsF-BG_{14}. In $(CsF)_2$-PG_{13}, the polar region comprises a $-Cs^+-F^-$ double layer derived from the rock salt structure (Figure 3a), but the configuration is distorted from the ideal structure because of interactions with PG_{13} from above and below. A similar, but less distorted, $-Cs^+-F^-$ double layer is observed in the $(CsF)_2$-Br_2 intercalation compound.[55] In contrast, the polar layer in CsF-BG_{14} contains six-membered rings of Cs^+ and F^- displaying the distorted boat conformation of a cyclohexane molecule, where each ring is capped above and below by two O atoms from BG_{14}. The BG_{14} molecules bridging the polar layers are tilted with respect to the *c*-axis, which contrasts with the perpendicular alignment of PG_{13}. Comparison of the BVS values for $(CsF)_2$-PG_{13} (1.01) and CsF-BG_{14} (1.07) suggests that the Cs^+ in CsF-BG_{14} is slightly over-coordinated relative to that in $(CsF)_2$-PG_{13} (Table S2, Supporting Information).

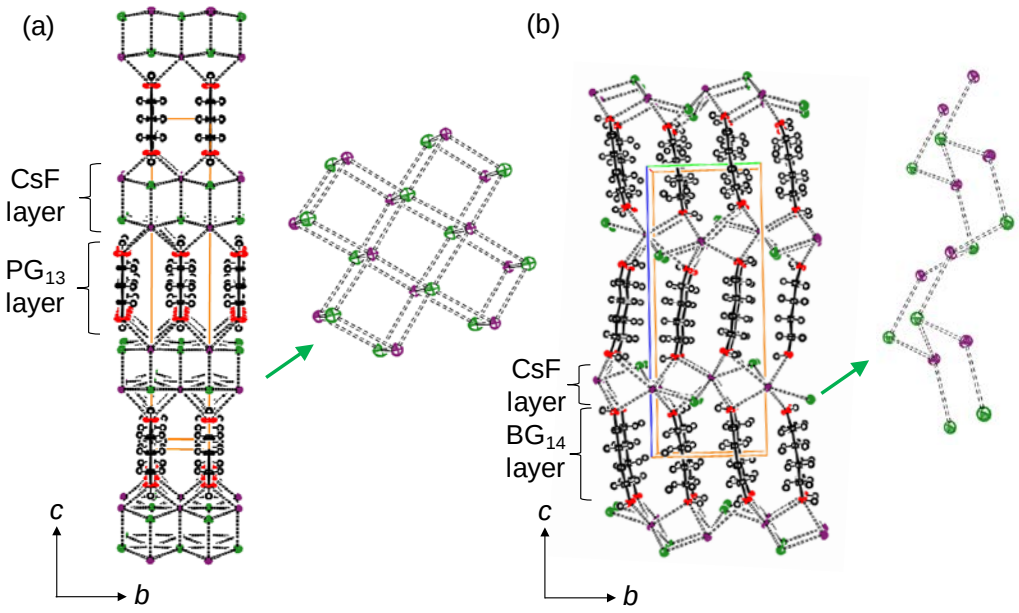

Figure 3. Packing diagrams of (a) $(CsF)_2$-PG_{13} viewed along the *a*-axis and (b) CsF-BG_{14} along the *a*-axis. Atom colors: C and H, black; O, red; F, green; Cs and Rb, purple. Hydrogen bonding is not shown.

Figure 4 shows the coordination environment of F^- in $(CsF)_2$-PG_{13} and CsF-BG_{14}. The F^- ion in CsF-BG_{14} is coordinated to three Cs^+ ions and two H atoms belonging to the OH groups of different BG_{14} molecules in a manner similar to that of the F^- in CsF-EG (Figure 2a) and F1 in $(RbF)_5$-$(EG)_4$ (Figure 2b). However, the F^- environment in $(CsF)_2$-PG_{13} is unique and consists of one H atom from an OH group and five Cs^+ ions arranged in a distorted octahedral manner. The five $Cs^+\cdots F^-$ contacts [$Cs^+\cdots F^-$ distances of 2.912(4) and 3.0623(5) Å] are included in a rock salt-type framework that is slightly shorter along the *c*-axis and elongated along the *a*- and *b*-axes (cf. 3.004 Å for $Cs^+\cdots F^-$ in pure CsF).[51,52] The Cs···F contacts in CsF-BG_{14} of 2.9614(14), 3.0261(16), and 3.0742(14) Å deviate somewhat from that in CsF. The H···F distance of 1.69 Å in $(CsF)_2$-PG_{13} is the shortest among those of alkali metal fluoride-diol complexes in the present study (Table 3). Further interpretation pertaining to precise H-atom positions will require structure determination by neutron diffraction.

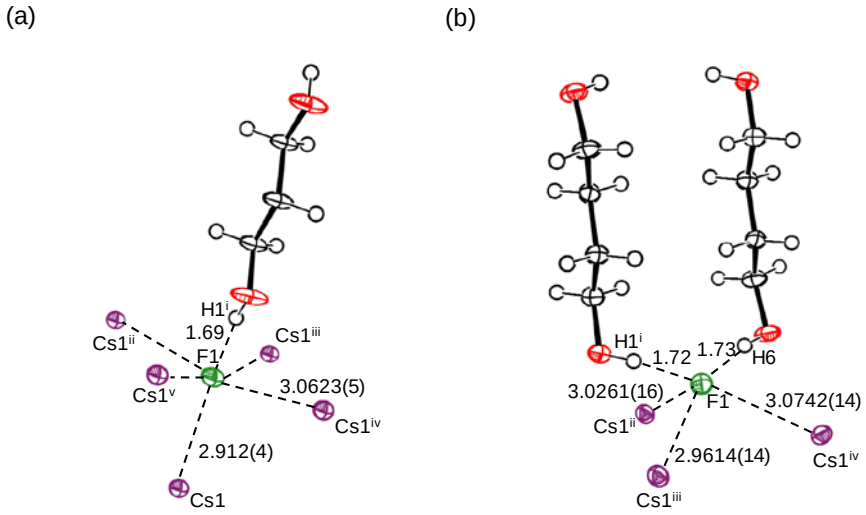

Figure 4. Coordination environment of F^- in (a) $(CsF)_2$-PG_{13} [symmetry code: (i) −x+1/2, −y+1, z; (ii) x−1/2, −y+1/2, −z+1/2; (iii) x+1/2, −y+1/2, −z+1/2; (iv) x+1/2, −y+3/2, −z+1/2; (v) x−1/2, −y+3/2, −z+1/2] and (b) CsF-BG_{14} [symmetry code: (i) −x+1, −y, −z+1; (ii) x, −y+1/2, z−1/2; (iii) x+1/2, −y+1/2, z−1/2; (iv) −x+1, −y+1, −z+1]. Thermal ellipsoids are shown at the 50 % probability level. Contacts are shown in Å

Fluoride ion interactions in CsF-EG, $(RbF)_5$-$(EG)_4$, $(KF)_5$-$(EG)_4$, $(CsF)_2$-PG_{13}, and CsF-BG_{14} were also investigated by Hirshfeld surface analyses.[56-59] This procedure analyzes intermolecular interactions by partitioning space in the crystal into regions where the electron distribution of a sum of spherical atoms in the molecule dominates the corresponding sum over the crystal. Figure 5 shows Hirshfeld surfaces and projections of normalized contact distances on the surface (d_{norm}) for F^- in the series of alkali metal fluoride-diol complex salts [see Figure S7 for $(KF)_5$-$(EG)_4$]. The red and blue colors on the d_{norm} surface correspond to intermolecular contacts that are shorter and longer, respectively, than the sum of their van der Waals surface radii. The white shading corresponds to the contacts around the sum of the van der Waals radii. The filtered two-dimensional (2D) fingerprints of the Hirshfeld surface, which are included in Figure 5, summarize the frequencies for each combination of d_e and d_i, where d_e and d_i are the distances from the surface to the nearest nucleus outside and inside the surface, respectively. The 2D plot shows the intermolecular interactions that are present in the crystal and indicates the relative surface area corresponding to each interaction.

The $F^-\cdots M^+$ and $F^-\cdots H$ interactions are observed around F^- in all complex salts [except for one of the two F^- ions in $(RbF)_5$-$(EG)_4$ which is surrounded by six Rb^+ cations(Figure 5b, left)] consistent with the contacts described in Figures 2 and 4. The color mapping suggests shorter $F^-\cdots H$ than $F^-\cdots M^+$ interactions based on the van der Waals interaction sums. The $F^-\cdots M^+$ interactions lie in a narrow range d_i = 1.2 to 1.4 Å, whereas the $F^-\cdots H$ interactions exhibit a wider range of d_i values. The $F^-\cdots H$ interactions contribute significantly to the d_{norm} surface in all cases (76.0, 68.6, 48.4 and 84.7% in CsF-EG, $(RbF)_5$-$(EG)_4$, $(CsF)_2$-PG13, and CsF-BG_{14}, respectively) suggesting the dominance of $F^-\cdots H$ contacts in the F^- coordination environment. Even in $(CsF)_2$-PG_{13}, where F^- contacts five Cs^+ and only one H atom, the $F^-\cdots H$

contribution to the surface equals 48.4%. Similarly strong $F^{-}\cdots H$ interactions in various F^{-} salts were suggested by Hirshfeld surface analyses in an earlier work.[60]

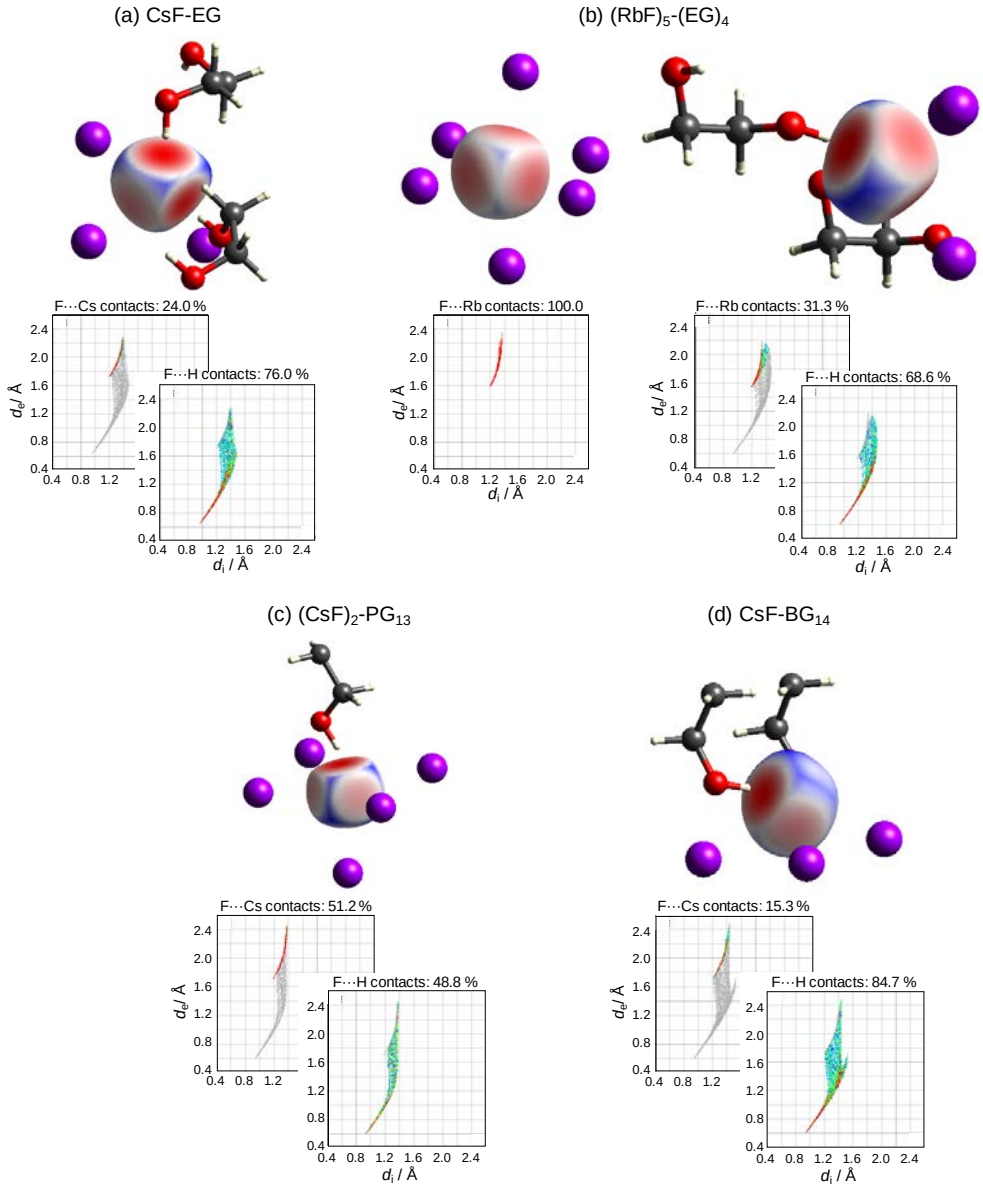

Figure 5. Hirshfeld surface analyses [projection of d_{norm} and filtered 2D fingerprint plots (F···Cs, F···Rb, and F···H)] of F^{-} in (a) CsF-EG, (b) $(RbF)_5$-$(EG)_4$, (c) $(CsF)_2$-PG_{13}, and (d) CsF-BG_{14}. The data shown for $(CsF)_2$-PG_{13} were calculated based on the ordered structure. Some carbon atoms in PG_{13} and BG_{14} are omitted for clarity. See Figure S7 for the $(KF)_5$-$(EG)_4$ and $(CsF)_2$-PG_{13} results based on a disordered model.

Infrared spectroscopic analyses. The frequency of the O–H stretching mode in alcohols is known to shift according to the strength of the H···A (A = hydrogen bond acceptor) interaction.[37,61] The O–H stretching mode of the powdered samples of CsF-EG, $(RbF)_5$-$(EG)_4$, $(KF)_5$-$(EG)_4$, $(CsF)_2$-PG_{13}, and CsF-BG_{14} was investigated by IR spectroscopy. For the preparation of these complex salts, the alkali metal fluoride and the corresponding diol were mixed in difluorobenzene to complete the reaction, and the solvent was removed under vacuum. The frequencies of absorption bands in the following discussion are represented by the values rounded off to the nearest ten wavenumbers because of their broadness.

Figure 6a shows IR spectra of CsF-EG, $(RbF)_5$-$(EG)_4$, $(KF)_5$-$(EG)_4$, and EG between 3800 and 2300 cm^{-1}, where absorption bands above 3000 cm^{-1} are assigned to the OH stretching mode of EG. The absorption peaks for CsF-EG at 3060 cm^{-1}, $(RbF)_5$-$(EG)_4$ at 3060 cm^{-1}, and $(KF)_5$-$(EG)_4$ at 3060 cm^{-1} are red-shifted by over 100 cm^{-1} compared to that for pure EG at 3170 cm^{-1}. Figure 6b shows the IR spectra of CsF-BG_{14}, BG_{14}, $(CsF)_2$-PG_{13}, PG_{13}, CsF-EG, and EG. The

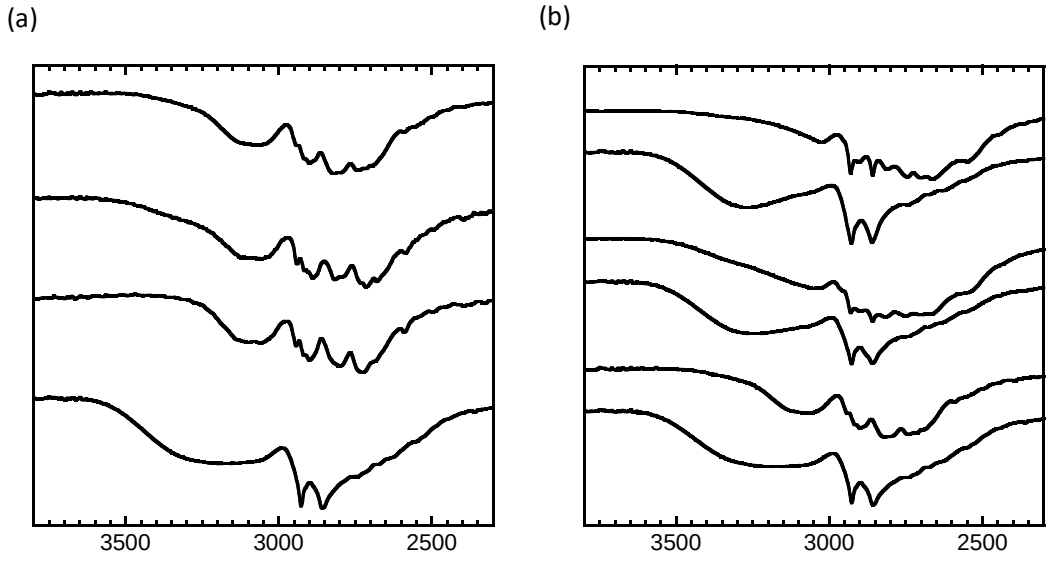

Figure 6. Infrared spectra of (a) CsF-EG, $(RbF)_5$-$(EG)_4$, $(KF)_5$-$(EG)_4$, and EG and (b) CsF-BG_{14}, BG_{14}, $(CsF)_2$-PG_{13}, PG_{13}, CsF-EG, and EG between 2300 and 3800 cm^{-1} at 25 °C.

absorption peaks for CsF-BG_{14} at 3030 cm^{-1} and $(CsF)_2$-PG_{13} at 3040 cm^{-1} are also red-shifted by over 200 cm^{-1} compared to that for pure BG_{14} at 3270 cm^{-1} and pure PG_{13} at 3240 cm^{-1}. These observations suggest that the O–H bond is weakened by the strong $F^{-}\cdots H$ interactions in these compounds. Pure diols are known to form inter- and intra-molecular hydrogen bonding in the liquid state.[62-67] For example, the red shift of the O–H stretching mode by intramolecular interactions is confirmed by comparing both vibrational frequencies of EG (free and hydrogen bonded) in a CCl_4 diluted solution (35.6 cm^{-1} shift).[68] Ab initio calculations for monomeric, dimeric, and trimeric EG also indicated a similar trend in clustering (113–183 cm^{-1} shift between EG and $(EG)_2$ and 186–211 cm^{-1} between EG and $(EG)_3$) at the M06-2X/6-31+G** level of theory.[69] By considering that these inter- and intra-molecular hydrogen bonding interactions already exist in pure diols, the large red-shift between the O–H stretching vibrational frequencies of pure diol and the corresponding fluoride complex suggests the significance of the $F^{-}\cdots H$ interaction. The sharper vibrational band of the diol complex salts than those in their pure diols are also consistent with fewer conformational states as a result of these strong interactions, although the difference in physical state (solid for complex salts and liquid for pure EG) also influences the peak shapes.

CONCLUSIONS

This work characterizes the properties of several alkali metal fluoride–diol complexes, which have not been previously studied. XRPD and XRF analyses establish that the reactivity of alkali metal fluorides and their solubilities in alcohols increase with increasing size of the alkali

metal cation, as expected from the relative Lewis basicities of the alkali metal fluorides. EG forms complex salts more easily than EtOH owing to its two OH groups.

The difference in alkali metal ion size produces different structural motifs in the CsF-EG and $(RbF)_5$-$(EG)_4$ complexes. The CsF-EG structure is of a layered type, whereas the $(RbF)_5$-$(EG)_4$ structure, which is isostructural with $(KF)_5$-$(EG)_4$, is columnar. The F^- ion coordination environment in CsF-EG is similar to one of the two F^- environments in $(RbF)_5$-$(EG)_4$ and is comprised of two short OH hydrogen contacts and three alkali metal cation contacts. The other F^- sites in $(RbF)_5$-$(EG)_4$ are surrounded by six Rb^+ ions in a distorted octahedral manner. The structural comparison of CsF-EG, $(CsF)_2$-PG_{13}, and CsF-BG_{14} demonstrates the effect of diol chain length on crystal packing and F^- coordination mode. Although all the glycol complexes form a layered structure, a distinct difference emerges in the diol bridging modalities. EG bridges two OH oxygen atoms within the same layer, whereas PG_{13} and BG_{14} bridge two OH oxygen atoms in different layers. The partially preserved rock salt-type CsF lattice observed in $(CsF)_2$-PG_{13} is characteristic of this series. The F^- in $(CsF)_2$-PG_{13} is coordinated by one OH hydrogen atom and five Cs^+ ions, whereas the F^- in CsF-BG_{14} is coordinated to two OH hydrogen atoms and three Cs^+ ions. Hirshfeld surface analysis reveals the $F^-\cdots H$ interaction is stronger than the $F^-\cdots M^+$ interaction of the F^- coordination sphere. The O–H bond weakening observed by IR spectroscopy also reflects the strengths of the $F^-\cdots H$ interactions in these complex salts.

Although fluorination reactions were not attempted in this work because of their limited solubilities to typical aprotic organic solvents, the structural data presented in these studies provide important information regarding the design of new reaction systems that involve the use of F^-. Further structural and physicochemical studies of F^--alcohol complexes are also suggested by this study.

EXPERIMENTAL

Apparatus and Materials. All non-volatile materials were handled under a dry Ar atmosphere in a glove box or under a dry air atmosphere in an open dry chamber (Daikin Industries, LTD.). The alkali metal fluoride salts, CsF (FUJIFILM Wako Pure Chemicals, >97.0% purity), RbF (Aldrich, 99.8% trace metal basis), and KF (FUJIFILM Wako Pure Chemicals, >99.0% purity) were dried at 423 K for 24 h prior to use. Dry EG (FUJIFILM Wako Pure Chemicals, <30 ppm water content), dry methanol (FUJIFILM Wako Pure Chemicals, <10 ppm water content), and dry EtOH (FUJIFILM Wako Chemicals, <50 ppm water content) were used without further purification. PG_{13} (FUJIFILM Wako Pure Chemicals, >97% purity), BG_{14} (FUJIFILM Wako Pure Chemicals, >98.0% purity), and 1,2-difluorobenzene (FUJIFILM Wako Pure Chemicals, >98.0% purity) were dried over 4A–1/16 molecular sieves (FUJIFILM Wako Pure Chemicals) for several days prior to use. The CsF-EG, $(RbF)_5$-$(EG)_4$, $(KF)_5$-$(EG)_4$, $(CsF)_2$-PG_{13}, and CsF-BG_{14} complex salts were prepared by directly mixing the alkali metal fluoride and diol in the appropriate stoichiometric ratios (see Supporting Information for detailed procedures). Their compositions were established by single-crystal X-ray diffraction.

Crystal growth. Single crystals of CsF-EG were grown on the walls of a glass vial from a tetraglyme mixture (CsF-EG:tetraglyme = 1:1) at room temperature. Single crystals of $(RbF)_5$-$(EG)_4$, $(KF)_5$-$(EG)_4$, $(CsF)_2$-PG_{13}, and CsF-BG_{14} were recrystallized by slowly cooling the corresponding saturated diol solution from an elevated temperature [$(RbF)_5$-$(EG)_4$: 70 °C, $(KF)_5$-$(EG)_4$: 80 °C, $(CsF)_2$-PG_{13}: 70 °C, and CsF-BG_{14}: 80 °C to room temperature. Suitable crystals were fixed in quartz capillaries in the glove box and sealed using an oxygen torch.

Single-crystal X-ray Diffraction. Single-crystal X-ray diffraction data was obtained using a R-axis Rapid II (Rigaku Corporation) diffractometer controlled by the RAPID AUTO 2.40 program.[70] Graphite-monochromated Mo Kα radiation (0.71073 Å) was used. Integration, scaling, and absorption corrections were performed using RAPID AUTO 2.40. The structure was solved using SIR-2014[71] and refined by SHELXL-97[72] linked to Win-GX.[73] Anisotropic displacement factors were introduced for all atoms except hydrogen. The H atoms were found in the difference Fourier synthesis after anisotropic refinement of the heavier atoms. The final refinement was carried out without constraining the C–H and O–H bonds. The Crystal Explorer 17.5 program was used for Hirshfeld surface analyses.[74] The PG_{13} disorder in $(CsF)_2$-PG_{13} was modeled on the averaged structure with partial occupancies and one of the disordered structures.

X-ray powder diffraction. X-ray powder diffraction patterns were collected in the Bragg-Brentano geometry using a Rigaku SmartLab diffractometer with Ni-filtered Cu-Kα radiation (40 kV and 30 mA) and a silicon strip high-speed detector (Rigaku D/teX Ultra 250). The powder sample was loaded on a glass plate in an air-tight cell with a Be window under dry Ar. The scan rate was 2 deg min^{-1}

Infrared spectroscopy. Infrared spectra were obtained with an Alpha II spectrometer equipped with an attenuated total reflection setup (Bruker Optics) in the open dry chamber under dry air at 25 °C. The sample was pressed onto the diamond prism. The spectral resolution was 4 cm^{-1}.

Spectroscopic and thermal analyses. Solution structures were analyzed by ^{1}H and ^{19}F NMR using a JNM-EC A600 NMR spectrometer equipped with an 14.0963-T cryomagnet. (JEOL Ltd.) at room temperature. A coaxial NMR tube was used with the sample placed in the inner tube and the deuterated solvent in the outer to prevent the interaction with the deuterated solvent. The ^{1}H and ^{19}F NMR spectra were acquired using probes operating at 600.172 and 564.726 MHz,

respectively. The 0.1 mol dm^{-3} EG solutions of KF, RbF, and CsF were prepared in the glove box by dissolving the corresponding alkali metal fluoride in EG.

X-ray fluorescence spectroscopy. Solubility was analyzed by X-ray fluorescence spectroscopy using an EDXL 300 (Rigaku Corporation) spectrometer at room temperature under a He atmosphere. Samples were loaded in a polypropylene container with a Prolene film window. The calibration line was obtained by dissolving a weighed amount of alkali metal fluoride in alcohols inside the glove box (three different concentrations for each alkali metal fluoride).

ASSOCIATED CONTENT

Supporting Information. The Supporting Information is available free of charge on the ACS Publications website at DOI: 10.1021/acs.inorg-chem.xxxxxxx. Synthetic, crystallographic, vibrational spectroscopic, NMR spectroscopic, and Hirshfeld surface analysis data (PDF)

Accession Codes.

CCDC 1983993-1983997 (CsF-BG_{14}: 1983993, CsF-EG: 198394, $(CsF)_2$-PG_{13}: 198395, $(KF)_5$-$(EG)_4$: 1983996, and $(RbF)_5$-$(EG)_4$: 1983997) contain the supplementary crystallographic data for this paper. These data can be obtained free of charge via www.ccdc.cam.ac.uk/data_request/cif, or by emailing data_request@ccdc.cam.ac.uk, or by contacting The Cambridge Crystallographic Data Centre, 12 Union Road, Cambridge CB21EZ, UK; fax: +44 1223 336033.

AUTHOR INFORMATION

Corresponding Author

*E-mail: k-matsumoto@energy.kyoto-u.ac.jp

ORCID

Kazuhiko Matsumoto: 0000-0002-0770-9210

Notes

The authors declare no competing financial interests.

ACKNOWLEDGMENT

This work was partly supported by JSPS KAKENHI Grant Number 17K14544.

REFERENCES

(1) Christe, K. O.; Wilson, W. W.; Wilson, R. D.; Bau, R.; Feng, J. A. Syntheses, properties, and structures of anhydrous tetramethylammonium fluoride and its 1-1 adduct with trans-3-amino-2-butenenitrile. *J. Am. Chem. Soc.* **1990**, *112*, 7619-7625.

(2) Seppelt, K. Does the Naked Fluoride Ion Exist? *Angew. Chem. Int. Ed.* **1992**, *31*, 292-293.

(3) Christe, K. O.; Jenkins, H. D. B. Quantitative measure for the "nakedness" of fluoride ion sources. *J. Am. Chem. Soc.* **2003**, *125*, 9457-9461.

(4) Sun, H.; DiMagno, S. G. Anhydrous tetrabutylammonium fluoride, *J. Am. Chem. Soc*. **2005**, *127*, 2050-2051.

(5) Elias, S.; Karton-Lifshin, N.; Yehezkel, L.; Ashkenazi, N.; Columbus, I.; Zafani, Y. Synthesis, characterization, and reactivity of thermally stable anhydrous quaternary ammonium fluorides. *Org. Lett*. **2017**, *19*, 3039-3042.

(6) Kornath, A.; Neumann, F.; Oberhammer, H. Tetramethylphosphonium fluoride: "Naked" fluoride and phosphorane. *Inorg. Chem*. **2003**, *42*, 2894-2901.

(7) Alič, B.; Tavčar, G. Reaction of N-heterocyclic carbene (NHC) with different HF sources and ratios – A free fluoride reagent based on imidazolium fluoride. *J. Fluorine Chem*. **2016**, *192*, 141-146.

(8) Gnann, R. Z.; Wagner, R. I.; Christe, K. O.; Bau, R.; Olah, G. A.; Wilson, W. W. Naked fluoride ion sources: Synthesis, characterization, and coupling reaction of 1-methylhexamethylenetetramine fluoride. *J. Am. Chem. Soc.* **1997**, *119*, 112-115.

(9) Mahjoub, A. R.; Zhang, X.; Seppelt, K. Reactions of the “naked” fluoride ion: Syntheses and structures of SeF_6^{2-} and BrF_6^-. *Chem. Eur. J.* **1995**, *1*, 261-265.

(10) Harmon, K. M.; Southwork, B. A.; Wilson, K. E.; Keefer, P. K. Synthesis and properties of diethyl 5,10-dihetera-5,10-dihydroindeno[2,1-a]indene-2,7-dicarboxylates. *J. Org. Chem.* **1993**, *58*, 7294-7295.

(11) Schwesinger, R.; Link, R.; Thiele, G.; Rotter, H.; Honert, D.; Limbach, H.; Männle, F. Stable phosphazenium ions in synthesis—an easily accessible, extremely reactive “naked” fluoride salt. *Angew. Chem., Int. Ed. Engl*. **1991**, *30*, 1372-1375.

(12) Christe, K. O.; Wilson, W. W.; Chirakal, R. V.; Sanders, J. C. P.; Schrobilgen, G. J. The hexafluorochlorate(V) anion, ClF_6^-. *Inorg. Chem.* **1990**, *29*, 3506-3511.

(13) Christe, K. O.; Sanders, J. C. P.; Schrobilgen, G. J.; Wilson, W. W. High-coordination number fluoro- and oxofluoro-anions; IF_6O^-, TeF_6O^{2-}, TeF_7^-, IF_8^- and TeF_8^{2-}. *J. Chem. Soc., Chem. Commun.* **1991**, 837-840.

(14) Mahjoub, A. R.; Seppelt, K. Preparation and structure of the IOF_6^- and TeF_7^- anions. *J. Chem. Soc., Chem. Commun.* **1991**, 840-841.

(15) Christe, K. O.; Dixon, D. A.; Mahjoub, A. R.; Mercier, H. P. A.; Sanders, J. C. P.; Seppelt, K. ; Schrobilgen, G. J.; Wilson, W. W. The IOF_6^- anion: the first example of a pentagonal bipyramidal AX_5YZ species. *J. Am. Chem. Soc.* **1993**, *115*, 2696-2706.

(16) Christe, K. O.; Dixon, D. A.; Sanders, J. C. P.; Schrobilgen, G. J.; Wilson, W. W. The hexafluorooxotechnetate(2-) anion: the first example of a multiply charged, pentagonal

bipyramidal, main-group element AX_5YZ species and the vibrational spectra of the $TeOF_5^-$ anion. *Inorg. Chem.* **1993**, *32*, 4089-4093.

(17) Christe, K. O.; Dixon, D. A.; Mercier, H. P. A.; Sanders, J. C. P.; Schrobilgen, G. J.; Wilson, W. W. Tetrafluorophosphite, PF_4^-, anion. *J. Am. Chem. Soc.* **1994**, *116*, 2850-2858.

(18) Zhang, X.; Groβ, U.; Seppelt, K. Flurocarbonate, $[FCO_2]^-$: Preparation and structure. *Angew. Chem., Int. Ed. Engl.* **1995**, *34*, 1858-1860.

(19) Drake, G. W.; Dixon, D. A.; Sheehy, J. A.; Boatz, J. A.; Christe, K. O. Seven-coordinated pnicogens. Synthesis and characterization of the SbF_7^{2-} and BiF_7^{2-} dianions and a theoretical study of the AsF_7^{2-} dianion. *J. Am. Chem. Soc.* **1998**, *120*, 8392-8400.

(20) Kornath, A.; Kadzimiraz, D.; Ludwig, R. Trifluorosulfite anion, SOF_3^-. *Inorg. Chem.* **1999**, *38*, 3066-3069.

(21) Lehmann, J. F.; Schrobilgen, G. J. Synthesis and characterization of salts containing the $BrO_3F_2^-$ anion; a rare example of a bromine(VII) species. *J. Am. Chem. Soc.* **2005**, *127*, 9416-9427.

(22) Brock, D. S.; Mercier, H. P. A.; Schrobilgen, G. J. $XeOF_3^-$, an example of an AX_3YE_2 valence shell electron pair repulsion arrangement; syntheses and structural characterizations of $[M][XeOF_3]$ (M = Cs, $N(CH_3)_4$). *J. Am. Chem. Soc.* **2010**, *132*, 10935-10943.

(23) Christe, K. O.; Curtis, E. C.; Dixon, D. A.; Mercier, H. P. A.; Sanders, J. C.; Schrobilgen, G. J. The pentafluoroxenate(IV) anion, XeF_5^-: the first example of a pentagonal planar AX_5 species. *J. Am. Chem. Soc.* **1991**, *113*, 3351-3361.

(24) Boatz, J. A.; Christe, K. O.; Dixon, D. A.; Fir, B. A.; Gnann, R. Z.; Mercier, H. P.; Schrobilgen, G. J. Synthesis, characterization, and computational study of the trans-$IO_2F_5^{2-}$ anion. *Inorg. Chem.* **2003**, *42*, 5282−5292.

(25) Lee, J. W.; Oliveira, M. T.; Jang, H. B.; Lee, S.; Chi, D. Y.; Kim, D. W.; Song, C. E. Hydrogen-bond promoted nucleophilic fluorination: concept, mechanism and applications in positron emission tomography. *Chem. Soc. Rev.* **2016**, *45*, 4638-4650.

(26) Engle, K. M.; Pfeifer, L.; Pidgeon, G. W.; Giuffredi, G. T.; Thompson, A. L.; Paton, R. S.; Brown, J. M.; Gouverneur, V. Hydrogen-bond promoted nucleophilic fluorination: concept, mechanism and applications in positron emission tomography. *Chem. Sci.* **2015**, ***6***, 5293-5302.

(27) Cox, D. P.; Terpinski, J.; Lawrynowicz, W. "Anhydrous" tetrabutylammonium fluoride: a mild but highly efficient source of nucleophilic fluoride ion. *J. Org. Chem.* **1984**, *49*, 3216-3219.

(28) Zaikin, P.; Dyan, O.; Evtushok, D.; Usoltsev, A.; Borodkin, G.; Karpova, E.; Shubin, V. Solvent-free fluorination of electron-rich aromatic compounds with F-TEDA-BF_4: Toward “dry” processes. *Eur. J. Org. Chem.* **2017**, ***2017***, 2469-2474.

(29) Sharma, R. K.; Fry, J. L. Instability of anhydrous tetra-n-alkylammonium fluorides. *J. Org. Chem.* **1983**, *48*, 2112-2114.

(30) Bouvet, S.; Pegot, B.; Marrot, J.; Magnier, E. Solvent free nucleophilic introduction of fluorine with [bmim][F]. *Tetrahedron Lett*. **2014**, *55*, 826–829.

(31) Pfeifer, L.; Engle, K. M.; Pidgeon, G. W.; Sparkes, H. A.; Thompson, A. L.; Brown, J. M.; Gouverneur, V. Hydrogen-bonded homoleptic fluoride–diarylurea complexes: Structure, reactivity, and coordinating power. *J. Am. Chem. Soc.*, **2016**, *138*, 13314-13325

(32) Yonezawa, T.; Sakamoto, Y.; Nogawa, K. K. Preparation of tetrabutylammonium fluoride–alcohol adducts as fluorination agents. *Jpn. Kokai. Tokkyo. Koho.*, 1994, JP06316551 A.

(33) Kim, D. W.; Jeong, H. J.; Lim, S. T.; Sohn, M. H.; Katzenellenbogen, J. A.; Chi, D. Y. Facile nucleophilic fluorination reactions using tert-alcohols as a reaction medium: significantly enhanced reactivity of alkali metal fluorides and improved selectivity. *J. Org. Chem*. **2008**, *73*, 957-962.

(34) Kim, D. W.; Ahn, D. S.; Oh, Y. H.; Lee, S.; Kil, H. S.; Oh, S. J.; Lee, S. J.; Kim, J. S.; Ryu, J. S.; Moon, D. H.; Chi, D. Y. A new class of S_N2 reactions catalyzed by protic solvents: Facile fluorination for isotopic labeling of diagnostic molecules. *J. Am. Chem. Soc*., **2006**, *128*, 16394-16397.

(35) Kim, D. W.; Jeong, H. J.; Lim, S. T.; Sohn, M. H. Facile nucleophilic fluorination of primary alkyl halides using tetrabutylammonium fluoride in a tert-alcohol medium. *Tetrahedron Lett*. **2010**, *51*, 432-434.

(36) Pupo, G.; Vicini, A. C.; Ascough, D. H.; Ibba, F.; Christensen, K. E.; Thompson, A. L.; Brown, J. M.; Paton, R. S.; Gouverneur, V. Hydrogen bonding phase-transfer catalysis with potassium fluoride: enantioselective synthesis of β-fluoroamines. *J. Am. Chem. Soc*. **2019**, *141*, 2878-2883.

(37) Chen, Z.; Tonouchi, Y.; Matsumoto, K.; Saimura, M.; Atkin, R.; Nagata, T.; Katahira, M.; Hagiwara, R. Partially naked fluoride in solvate ionic liquids. *J. Phys. Chem. Lett.* **2018**, *9*, 6662-6667.

(38) Gerken, M.; Boatz, J. A.; Kornath, A.; Haiges, R.; Schneider, S.; Schroer, T.; Christe, K. O. The ^{19}F NMR shifts are not a measure for the nakedness of the fluoride anion. *J. Fluorine Chem.* **2002**, *116*, 49-58.

(39) Kim, D. W.; Jeong, H. J.; Lim, S. T.; Sohn, M. H. Tetrabutylammonium tetra(tert-butyl alcohol)-coordinated fluoride as a facile fluoride source. *Angew. Chem. Int. Ed.* **2008**, *47*, 8404-8406.

(40) Libra, E. R.; Scott, M. J. Metal salen complexes incorporating triphenoxymethanes: efficient, size selective anion binding by phenolic donors with a visual report. *Chem. Commun.* **2006**, 1485–1487.

(41) Chen, C.H.; Leung, M. The nature of 6,6'-bis(triphenylamine) substituted BINOL as chromophoric and fluorogenic hybrid chemosensor for selective fluoride detection. *Tetrahedron* **2011**, *67*, 3924-3935.

(42) Ravikumar, I.; Lakshminarayanan, P. S.; Arunachalam, M.; Suresh, E.; Ghosh, P. Anion complexation of a pentafluorophenyl-substituted tripodal ureareceptor in solution and the solid state: selectivity toward phosphate. *Dalton Trans.* **2009**, *21*, 4160-4168.

(43) Li, M.; Wu, B.; Jia, C.; Huang, X.; Zhao, Q.; Shao, S.; Yang, X. J. An electrochemical and optical anion chemosensor based on tripodal tris(ferrocenylurea). *Chem. Eur. J.* **2011**, *17*, 2272-2280.

(44) Paul, M.; Adarsh, N. N.; Dastidar, P. Cull Coordination polymers capable of gelation and selective SO_4^{-2} separation. *Cryst. Growth Des.* **2012**, *12*, 4135-4143.

(45) Kormos, A.; Móczár, I.; Pál, D.; Baranyai, P.; Holczbauer, T.; Palló, A.; Tóth, K.; Huszthy, P. Unique fluoride anion complexation in basic media by 5,5-dioxophenothiazine bis(phenylurea) and bis(phenylthiourea). *Tetrahedron*, **2013**, *69*, 8142-8146.

(46) Babji, N. R.; McCusker, E. O.; Whiteker, G. T.; Canturk, B.; Choy, N.; Creemer, L. C.; De Amicis, C. V.; Hewlett, N. M.; Johnson, P. L.; Knobelsdorf, J. A.; Li, F.; Lorsbach, B. A.; Nugent, B. M.; Ryan, S. J.; Smith, M. R.; Yang, Q. NMR chemical shifts of trace impurities: Industrially preferred solvents used in process and green chemistry. *Org. Process. Res. Dev.* **2016**, *20*, 661-667

(47) Brown, I.D.; Altermatt, D. Bond-valence parameters obtained from a systematic analysis of the inorganic crystal structure database. *Acta. Crystallogr., Sect. B: Struct. Sci.* **1985**, *41*, 244–247.

(48) Brese, N.E.; Okeeffe, M. Bond-valence parameters for solids. *Acta. Crystallogr., Sect. B: Struct. Sci.* **1991**, *47*, 192–197.

(49) Fortes, A. D.; Suard, E. Crystal structures of ethylene glycol and ethylene glycol monohydrate. *J. Chem. Phys.* **2011**, *135*, 234501.

(50) Chopra, D.; Row, T. N. G.; Arunan, E.; Klein, R. A. Crystalline ethane-1,2-diol does not have intra-molecular hydrogen bonding: Experimental and theoretical charge density studies. *J. Mol. Struct.* **2010**, *964*, 126–131.

(51) Davey, W. P. Precision measurements of crystals of the alkali halides. *Phys. Rev.* **1923**, *21*, 143-161.

(52) Karo, A. M. Lattice vibrations in alkali halide crystals. II. Potassium and rubidium halides; cesium fluoride. *J. Chem. Phys.* **1960**, *33*, 7-20.

(53) Bondi, A. van der Waals volumes and radii. *J. Phys. Chem*. **1964**, *68*, 441−451.

(54) Kim, D. W.; Jeong, H.; Lim, S. T.; Sohn, M. Tetrabutylammonium tetra(tert-butyl alcohol)-coordinated fluoride as a facile fluoride source. *Angew. Chem.* **2008**, *120*, 8532–8534.

(55) Drews, T.; Marx, R.; Seppelt, K. Cesium fluoride–bromine intercalation compounds. *Chem. Eur. J.* **1996**, *2*, 1303-1307.

(56) Spackman, M. A.; Jayatilaka, D. Hirshfeld surface analysis. *Cryst. Eng. Comm.* **2009**, *11*, 19−32.

(57) McKinnon, J. J.; Jayatilaka, D.; Spackman, M. A. Towards quantitative analysis of intermolecular interactions with Hirshfeld surfaces. *Chem. Comm*. **2007**, *37*, 3814−3816.

(58) McKinnon, J. J.; Spackman, M. A.; Mitchell, A. S. Novel tools for visualizing and exploring intermolecular interactions in molecular crystals. *Acta. Crystallogr., Sect. B: Struct. Sci.* **2004**, *60*, 627−668.

(59) Hirshfeld, F. L. Bonded-atom fragments for describing molecular charge densities *Theor. Chim. Acta.* **1977**, *44*, 129−138.

(60) Cametti, M.; Rissanen, K. Highlights on contemporary recognition and sensing of fluoride anion in solution and in the solid state. *Chem. Soc. Rev.* **2013**, *42*, 2016-2038.

(61) Barlow, S. J.; Bondarenko, G. V.; Gorbaty, Y. E.; Yamaguchi, T.; Poliakoff, M. An IR study of hydrogen bonding in liquid and supercritical alcohols. *J. Phys. Chem. A* **2002**, *106*, 10452-10460.

(62) Frey, H.; Ha, T.–K.; Meyer, R.; Günthard, Hs. H. Ethylene glycol: Infrared spectra, Ab initio calculations, vibrational analysis and conformations of 5 matrix isolated isotopic modifications. *Chem. Phys.* **1977**, *25*, 271-298.

(63) Buckley, P.: Giguère, P. A. Infrared studies on rotational isomerism. I. Ethylene glycol. *Can. J. Chem.* **1967**, *45*, 397-407.

(64) Karas, L. J.; Batista, P. R.; Viessar, R. V.; Tormena, C. F.; Ritter, R.; de Oliveira, P. R. Trends of intramolecular hydrogen bonding in substituted alcohols: a deeper investigation. *Phys. Chem. Chem. Phys*. **2017**, *19*, 16904-16913.

(65) Shagidullin, Rif. R.; Chernova, A. V.; Plymavatyi, A. Kh.; Shagidullin, R. R. ntramolecular hydrogen bonding and conformation of 1,3-propanediol. *Struct. Mol.* **1991**, *40*, 1993-1999.

(66) Fishman, E.; Chen, T. L. An investigation of the hydrogen bonding characteristics of butanediols. *Spectrochim. Acta. A*, **1969**, *25*, 1231-1242.

(67) Shagidullin, Rif. R.; Chernova, A. V.; Shagidullin, R. R. Intramolecular hydrogen bonds and conformations of the 1,4-butanediol molecule. *Russ. Chem. Bull*. **1993**, *42*, 1505-1510.

(68) Ma, X.; Wang, J. Differentiating subtle variation of weak intramolecular hydrogen bond in vicinal diols by linear infrared spectroscopy. *J. Phys. Chem. A* **2009**, *113*, 6070-6076.

(69) Kumar, R. M.; Baskar, P.; Balamurugan, K.; Das, S.; Subramanian, V. On the perturbation of the H-bonding interaction in ethylene glycol clusters upon hydration. *J. Phys. Chem. A* **2012**, *116*, 4239-4247.

(70) *RAPID AUTO*, *version 2.40*; Rigaku Corporation: Tokyo, Japan, 2006.

(71) Burla, M. C.; Caliandro, R.; Carrozzini, B.; Cascarano, G. L.; Cuocci, C.; Giacovazzo, C.; Mallamo, M.; Polidori, A. G. Crystal structure determination and refinement *via SIR2014*. *J. Appl. Crystallogr* **2015**, *48***,** 306-309.

(72) Sheldrick, G. M. A short history of SHELX. *Acta. Crystallogr. Sect. A: Found. Crystallogr.* **2008**, *64*, 112-122.

(73) Farrugia, L. J. *WinGX* suite for small-molecule single-crystal crystallography. *J. Appl. Crystallogr.* **1999**, *32*, 837-838.

(74) Wolff, S. K.; Grimwood, D. J.; McKinnon, J. J.; Turner, M. J.; Jayatilaka, D.; Spackman, M. A. CrystalExplorer 17.5; University of Western Australia: Crawley, Australia, 2012.

SYNOPSIS TOC

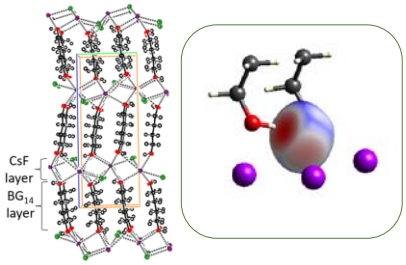

This work investigates interactions of F^- with diols in alkali metal fluoride-diol complexes by basic reactivity and solubility tests, X-ray diffraction and infrared spectroscopy. The differences in alkali metal ion size and diol chain length produce various structural motifs of the F^--diol complex salts, and $F^-\cdots H$ interaction is more dominant than the $F^-\cdots M^+$ interaction in F^- coordination environment.